Research Article Vol. 3, No. 11 / 15 November 2020 / OSA Continuum 3176

Coherent beam combining of multipass thin-disk lasers with active phase control

MICHAEL ZWILICH AND BENJAMIN EWERS*

German Aerospace Center (DLR), Institute of Technical Physics, Pfaffenwaldring 38-40, 70569 Stuttgart, Germany
*benjamin.ewers@dlr.de

Abstract: Coherent beam combining and the development of thin-disk lasers have provided the ability to increase the output power of solid-state laser systems. Here, coherent beam combining by active phase control of one multipass thin-disk laser amplifier and one similar multipass setup is demonstrated with powers below 100 mW. Piston phase disturbances are measured via optical heterodyne detection and compensated for by piezo mirrors. For one double pass over the disk, a root mean square phase error of $\lambda/69$ was achieved. Mechanical vibrations < 5 kHz inside the multipass setup caused by the water cooling of the disk are the main source of phase noise. Thermal effects by the pumping diodes with 1 kW of optical power are negligible.

1. Introduction

High-power lasers are used for material processing as well as scientific and directed energy purposes, where typical laser geometries include slab, fiber and thin-disk lasers. Each of these geometries makes use of a large surface-to-volume ratio, which allows for more efficient heat removal compared to the archetypal rod geometry. Nonetheless, with higher pump powers thermal effects again begin to play a role.

In a thin-disk laser system the active medium is shaped as a disk with a thickness of a few hundred µm. The disk's backside is mounted directly to a heat sink. Because of the low thickness of the disk compared to its diameter, there is virtually no heat flow radial to the laser beam axis. This reduces thermal effects limiting output power and beam quality [1]. Thin-disk laser systems comprising a single disk have reached output powers of 12 kW [2]. With higher pump powers the weak thermal lensing degrades achievable beam quality [3]. Compensating the curvature of the disk with a deformable mirror has led to output powers of up to 4 kW with $M^2 < 1.2$ [4].

Similar to thin-disk lasers fiber lasers are capable of generating beams with high power and/or good beam quality. This is due to the waveguide nature of the fiber and the efficient heat dissipation. In single mode operation, output powers of up to 20 kW have been claimed [5], but unfortunately no beam quality measurements have been published. Near diffraction limited output has been achieved with powers of up to 5 kW [6–8]. Power scaling of near diffraction limited output from a single fiber laser is affected by thermal [9] and non-linear effects [10,11].

Coherent beam combining is an approach, which allows to increase output power while maintaining beam quality [12]. Typically, an oscillator's beam is split up into multiple channels, which pass through amplifiers in parallel. By controlling each channel's piston phase, they can be combined interferometrically yielding an output beam with the sum of their powers. Coherent beam combining mitigates the complex thermal management of a single amplifier setup, as it allows power scaling by adding multiple simple amplifiers in parallel. Complexity arises from the need to compensate phase differences between channels, for example introduced by mechanical vibrations, to maintain constructive interference. These disturbances are compensated for by phase shifting elements, such as piezo mirrors or electro-optic modulators.

#404658 https://doi.org/10.1364/OSAC.404658
Journal © 2020 Received 6 Aug 2020; revised 23 Sep 2020; accepted 24 Sep 2020; published 2 Nov 2020

OSA CONTINUUM

By incoherently superimposing multiple fiber laser sources, multimode operation with an output power of about 100 kW and M^2>47 has been realized [13]. In contrast, coherent beam combining of slab amplifiers has enabled 100 kW output with very good beam quality of three times that of a diffraction limited beam [14]. Near diffraction limited output has been demonstrated with average powers of up to 10 kW (M^2<1.2) [15]. Coherent beam combining is also used with bulk amplifiers, mainly in pulsed operation [16–18].

In this paper we demonstrate coherent beam combining of two beams passing through a multipass thin-disk laser amplifier and a similar multipass setup respectively. In doing so, we focus on analyzing occurring phase noise and establishing a control system for compensation rather than achieving high output power or high gain. To ensure a stable phase relationship between both beams an active control system is implemented. Optical heterodyne detection is used to measure the phase of the beams passing through each multipass setup. Piston phase disturbances are compensated for by moving mirrors attached to piezo actuators.

2. Experimental setup

2.1. Multipass thin-disk laser amplifier

In this section the optical setup for coherently combining two beams as well as a multipass setup using a thin-disk for amplification is presented. A simplified sketch of the oscillator-amplifier configuration is depicted in Fig. 1. A diode pumped solid state laser (*Integrated Optics 1030 NM SLM Laser*) with an emission wavelength λ = 1029.5 nm, 0.2 pm linewidth and 400 mW cw output power is used as oscillator. A Faraday isolator is used to prevent back reflections. The oscillator's beam passes into an acousto-optical modulator (AOM) generating a 100 MHz frequency shifted first order beam, which is used for phase measurements. The non-diffracted zero order beam and the first order beam are coupled into polarization maintaining fibers to enable flexible beam guiding on the optical table.

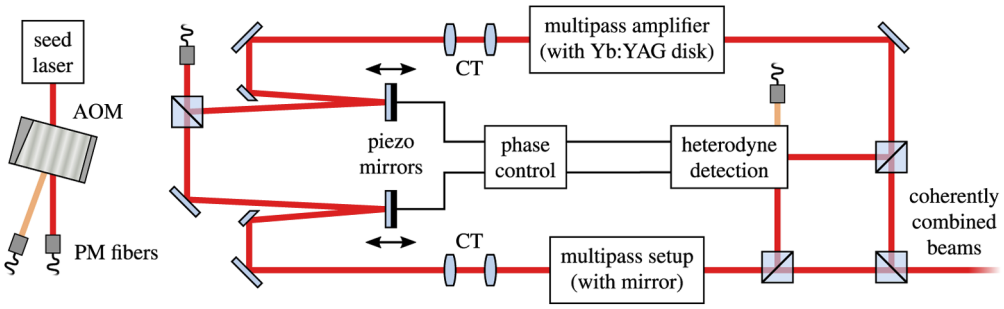

Fig. 1. Simplified schematic experimental setup. CT: collimating telescope.

After leaving the fiber the zero order beam is split up by a beam splitter cube with equal power splitting ratio. Each beam passes symmetric multipass setups (see Fig. 2). They differ insofar as one is a fully functional thin-disk amplifier with a Yb:YAG disk, whereas in the other setup there is a dielectric mirror at the corresponding location. The Yb:YAG disk has a diameter of 15 mm, a thickness of 200 µm and a dopant concentration of about 10 at.%. The disk is mounted on a 2 mm thick diamond heat sink, which can be cooled by turbulent water flow (20 °C) from the backside. The disk is optically pumped by four indium gallium arsenide diode stacks with λ = 940 nm. Their beams are combined by a homogenizer to form a hexagonally shaped near flat top intensity profile with an overall power of up to 1.8 kW and a beam diameter of 8.4 mm. This pump beam is imaged onto the disk twelve times by a set of prisms and parabolic mirrors.

OSA CONTINUUM

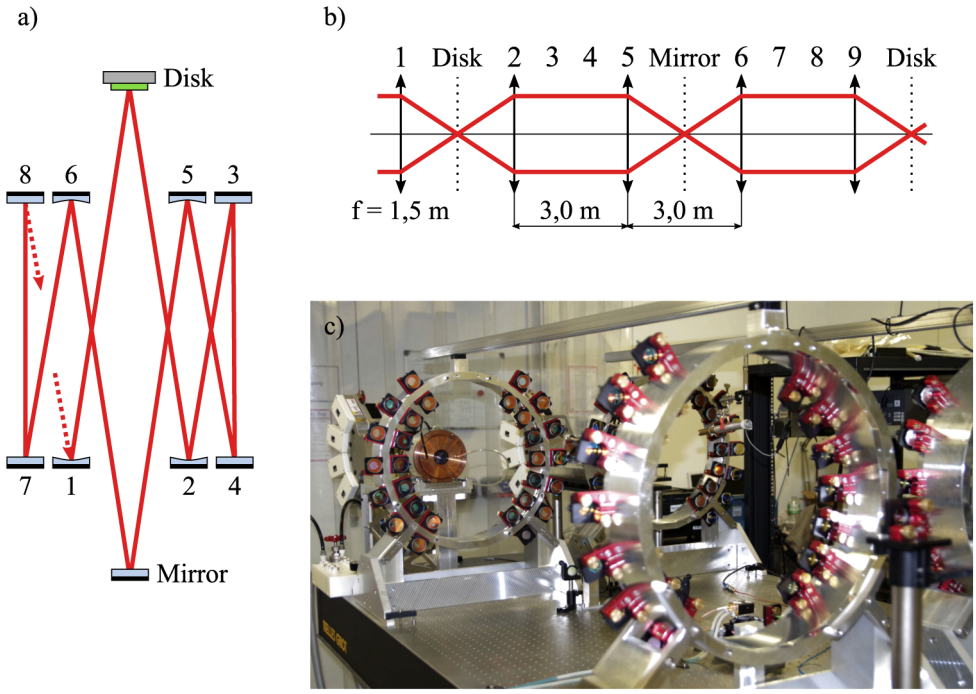

Fig. 2. a) Mirror arrangement for one disk double pass (top view). The water cooling on the disk's rear side and the pump beams are not shown. By slightly adjusting mirror 8 the beam can leave the amplifier or be redirected to mirror 9 for another disk pass. b) Unfolded beam path (simplified to geometric optics). The beam is repeatedly imaged onto the disk. c) Photograph of the used multipass thin-disk laser amplifiers.

Four concave mirrors with focal lengths of $f = 1.5$ m form a relay optic and image the incoming seed beam onto the disk (see Fig. 2(a) and (b)) [19]. Four additional plane mirrors fold the beam path. By rotating this setup needed for one double pass through the disk the mirror arrangement for multiple passes is generated, which can be seen as the two ring shaped structures in Fig. 2(c). The curved mirrors are mounted on the inner sides, the plane ones on the outer sides of the rings. With this setup up to seven double passes through the disk can be realized.

With an optical pump power of about 600 W and three disk double passes a total amplification of $G = 1.3$ was achieved. The low input power of 75 mW results in a low extraction efficiency.

2.2. Phase measurement and control

The phase control loop for every beam consists of three major building blocks. Firstly, phase changes relative to a reference are measured via optical heterodyne detection. Secondly, based on the heterodyne signal a digital controller is used to calculate a control signal so that the phase change of the beam with respect to the reference is minimized. Thirdly, a piezo actuator with a mirror attached to it is used to convert the control signal into a movement, thereby adjusting the optical path length and compensating piston phase disturbances. By employing such phase control loops the phase changes of the outgoing beam of each multipass setup are minimized separately. Thus, a fixed relative phase relationship between them is established due to the common reference. With an additional static phase modulator the absolute phase difference of the beams can be adjusted manually. One phase shifter would be sufficient to achieve a constant phase difference between both beams and thus establish coherence. Here two piezo mirrors are

OSA CONTINUUM

used, which enables individual controlling and testing of each multipass setup. Additionally, this modular approach allows straightforward addition of further amplifiers.

To measure phase changes of the beams via optical heterodyne detection a fraction of each beam that passed through one of the multipass setups is combined with the frequency shifted optical reference created by the AOM. Superimposing each beam with this reference on a photo diode yields a phase-modulated electronic beating signal at their frequency difference of 100 MHz. Each beating signal's phase is a measurement of the ongoing change of the phase difference between the corresponding beam and the optical reference. With a phase comparator (*Analog Devices AD8302*) the beating signal is compared to the sinusoidal voltage signal driving the AOM. The phase comparator's output voltage is proportional (10 mV/deg) to the phase difference between these signals, thus extracting each beam's phase change over time from the beating signal. Due to the symmetric phase to voltage characteristic, phase differences can be measured unambiguously as long as they do not exceed $-90° \pm 90°$ or $90° \pm 90°$.

Based on the measured phase difference a controller outputs a voltage, such that phase disturbances can be compensated with the piezo actuators. The controller is implemented digitally as a proportional-integral controller. The output is calculated recursively, thus eliminating integrator windup [20]. In every iteration it is checked, whether the calculated output would exceed the 16-bit limits of the digital analog converter. Due to integer arithmetic this would cause a sign change and therefore result in a sudden and great change in piezo actuator position. This might lead to instabilities caused by oscillations at the actuators resonance frequency or repeated jumping back and forth. To prevent this, the output in these cases is set back to the middle of the actuator's range.

The controller is implemented on a field-programmable gate array (FPGA). A *Kintex-7 XC7K325T* is used together with a *NI-5783* I/O module. The output signal of the phase comparator is sampled at 100 MHz. For evaluation purposes it is advisable to create two signal paths. Along one the controller's output is computed and along the other remaining phase disturbances are assessed. Along the control signal path the sampling rate is reduced to 100 kHz by evaluating only one in every 1000 samples. This, of course introduces aliasing. But the input signal is dominated by frequencies below 10 kHz, making these distortions negligible. In comparison, low pass filtering before decimation introduced time delays, which had a significant negative impact on the control loop performance. In contrast, along the second signal path such delay introducing filters can be used, because evaluating the error is not time critical. Here, the input signal is low pass filtered and decimated by a cascaded integrator-comb filter (CIC filter). The amplitude drop in the passband is compensated by a finite impulse response filter (FIR filter). This filter combination reduces the sampling rate to 250 kHz and has a low pass filtering characteristic with a cutoff frequency of 100 kHz. With this division the remaining phase noise can be evaluated regardless of possible aliasing or filtering of the signal used to compute the controller output.

Two piezo elements with mirrors attached to each of them are used as phase shifting elements. The length of the beam path through multipass setup 1 (with Yb:YAG disk) is changed by a piezo stack with a maximum free stroke displacement of 19.6 µm at 75 V and a resonance frequency of 63 kHz (*Thorlabs PK2FQP2*). For multipass setup 2 a *PI P-842.10* with a maximum displacement of 15 µm at 100 V and a resonance frequency of 18 kHz is used. The output voltage of the controller (max. 2 V) is amplified by a voltage amplifier and by a power amplifier to match the specified maximum voltage range of the piezo elements.

Before phase noise measurements are discussed, a software defined radio (SDR) is introduced as a second phase measurement device. The SDR used is a repurposed DVB-T dongle consisting of a *Rafael Micro R820T* tuner chip and a *Realtek RTL2832U* as demodulator. It also processes the phase modulated beating signal recorded by the photo diode, which is then digitized and

OSA CONTINUUM

demodulated into a phase (I) and a quadrature phase component (Q). The optical phase is calculated as the inverse tangent of the ratio of Q and I by a *LabVIEW* extension [21].

Phase noise measurements by the controller's error signal path (using the phase comparator) and the SDR are in good agreement with each other for frequencies greater than 20 Hz. For smaller frequencies phase noise measurements by the SDR show significantly higher spectral components, because there is no synchronization between modulation frequency source and demodulation frequency source, which introduces signal distortions at low frequencies. Therefore, root mean square values calculated from SDR measurements can be seen as an upper limit of the actual phase noise. Furthermore, typical time delays reported for SDR are in the range of tens of milliseconds [22], rendering it unsuitable for real time control purposes. Despite these limitations, due to its unrestricted measurement range, the SDR can be used to estimate phase noise even with amplitudes of multiple optical wavelengths, for example without active phase control.

As noted above the phase comparator's unambiguous measurement interval is limited to $90° \pm 90°$. With the 50 Ω input impedance of the controller's analog digital converter, the phase comparator cannot output the current necessary to generate the maximum voltage corresponding to 0° phase difference. The characteristic curve flattens and further reduces the measurement range from 180° to 114°. As long as phase deviations are small, no distortions occur and they can be measured accurately. If however phase disturbances exceed the interval, real phase noise is underestimated. In these cases root mean square values computed from phase comparator measurements can be seen as a lower boundary, whereas values calculated from SDR measurements are an upper boundary. This can be seen in Fig. 5. For one and two double passes phase noise with activated control loop is small and the OPD_{rms} (optical path difference) values are computed from the controller error. For three and four double passes it is given as the mean between the two phase noise measurements with a corresponding uncertainty interval.

3. Results

In order to evaluate phase noise it is initially measured without active phase control. As described in Sec. 2.2 these measurements are performed by using the SDR to process the beating signal from the heterodyne measurement since phase differences of multiple optical wavelengths can occur.

On the left hand side in Fig. 3 one second long recordings of phase noise for different surrounding conditions are shown. The first subplot (top left, blue) depicts the phase noise generated mainly by air flow and sound waves caused by laboratory equipment such as flow box and cooling fans. This results in a root mean square optical path difference of OPD_{rms} = 39 nm. As is evident from the time signals, turning on the water cooling of the laser disk (middle, orange) has a major impact on phase noise. Excited mechanical vibrations increase OPD_{rms} to 195 nm. Activating the pumping diodes (bottom, green) with $P \approx 1$ kW had little effect and resulted in OPD_{rms} = 201 nm. Similar observations regarding the negligible phase shifting effect of pumping diodes compared to water cooling have been made for fiber amplifiers [23].

The right hand side of Fig. 3 shows an analysis of the spectral properties of the occurring phase noise under different circumstances. In all cases most phase noise occurs within the frequency range between 30 Hz and 200 Hz. Additionally, there are considerable spectral components around 4.5 kHz. These frequency bands are characteristic for the mechanical setup used (see Fig. 2) and mainly defined by its eigenfrequencies. The response to a manually induced impulse at one of the ring-shaped structures shows optical path difference changes in the same frequency regions, indicating that mechanical vibrations are indeed the main cause of phase noise in this setup. Furthermore, it can be seen that the water cooling generates phase disturbances with frequencies of up to approximately 4 kHz. In contrast, the pumping diodes introduce smaller disturbances at lower frequencies of up to 100 Hz.

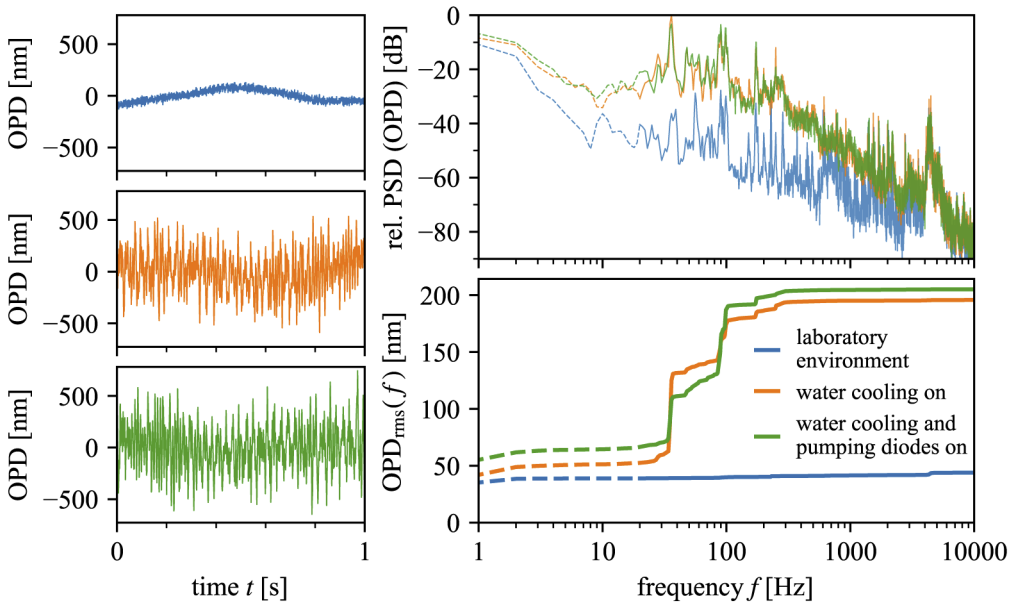

Fig. 3. Phase noise for one double pass through the disk without phase control. The power spectral density (PSD) of the optical path difference (OPD) is normalized to the highest spectral component. Dashed lines indicate frequency intervals where phase noise is overestimated (see Sec. 2.2).

As described in Sec. 2.2 low frequency phase noise <20 Hz is overestimated by the lacking synchronization of the SDR. This is indicated by dashed lines.

A useful metric, which can be calculated from the spectral components, is the frequency dependent root mean square of the optical path difference $\mathrm{OPD}_{\mathrm{rms}}(f)$. It is equivalent to low pass filtering the time signal with a cutoff frequency f and computing $\mathrm{OPD}_{\mathrm{rms}}$ for each frequency. However, it can be expressed as the cumulative sum of the absolute square of the spectral components $X_k = \mathcal{F}[\mathrm{OPD}(t)]$:

$$\mathrm{OPD}_{\mathrm{rms}}(f) = \frac{1}{N}\sqrt{\sum_{k=-fNT}^{fNT} |X_k|^2}. \tag{1}$$

N is the number of samples and T the inverse of the sampling rate. This analysis is depicted on the lower right hand side of Fig. 3. The rise in overall phase noise due to water cooling and pumping diodes can be attributed to disturbances with frequencies from 30 Hz to 200 Hz. For larger frequencies there is little change in $\mathrm{OPD}_{\mathrm{rms}}$ and the values approach the ones calculated from the time signal.

By activating the phase control loop disturbances can be compensated, diminishing the change in optical path difference between beam and reference over time. Using a sampling rate of 100 kHz yielded the best results, although the true repositioning speed of the piezo mirrors is certainly lower given their resonance frequencies and their amplifiers bandwidth. Figure 4 shows the effect of the control loop in time and frequency domain for one double pass through the laser disk. Disturbances of up to about 2 kHz can be damped reducing phase noise to $\mathrm{OPD}_{\mathrm{rms}} = 19\ \mathrm{nm} = \lambda/54$ (compared to $201\ \mathrm{nm} = \lambda/5$ without phase control). At higher frequencies phase noise increases compared to the measurement without activated phase control. This is likely caused by positive feedback due to time delays introduced by the electrical amplifiers

OSA CONTINUUM

driving the piezo actuators in combination with the remaining vibrations at 4.5 kHz, that are characteristic for the used mechanical setup.

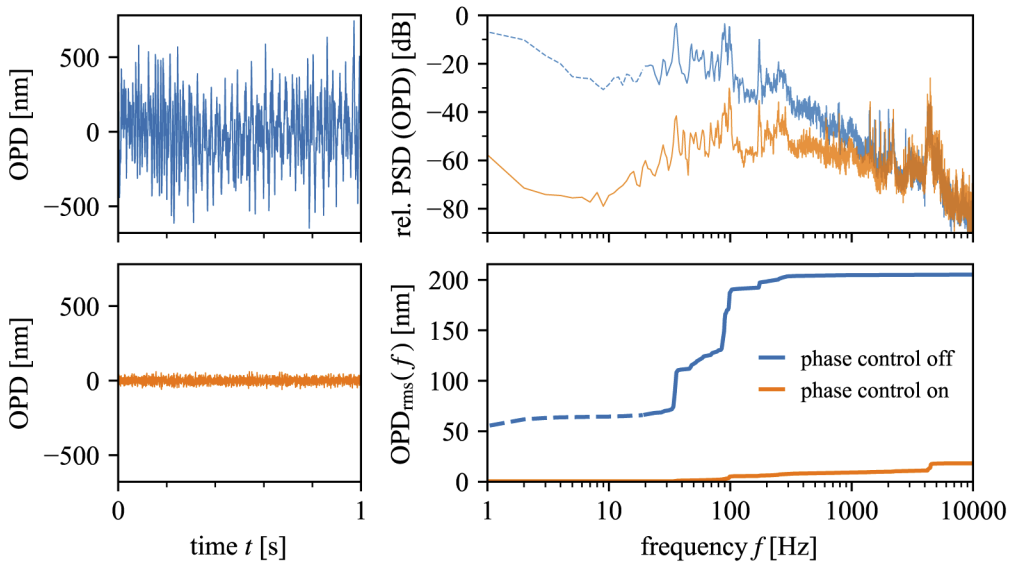

Fig. 4. Reduction of phase noise for one double pass through the disk with water cooling and pumping diodes on. Dashed lines indicate overestimation of phase noise.

Phase noise with and without control loop for multiple passes through the disk are summarized in Fig. 5. Without phase control (light shade) phase noise increases linearly with the number of passes through the thin-disk. This again indicates that mechanical vibrations inside the multipass setup are the main cause of phase noise, because every displacement leads to an optical phase difference that is proportional to the number of passes through the disk. Stable phase control (dark shade) was achieved for up to four double passes through the thin-disk. This means that over the course of several seconds no disturbances occurred that exceeded the control range. The corresponding $\mathrm{OPD_{rms}}$ values are given as annotations on top of the bars. Since mostly lower frequencies (30 Hz to 200 Hz) are damped (see Fig. 4), disturbances at 4.5 kHz are the major contributor to phase noise, especially for a higher number of passes through the disk.

The rings, on which the mirrors for the multipass amplifier are mounted, can be connected with five rods. With this modified setup the same measurements were carried out. The stiffening changes the resonating properties of the mechanical setup, which results in a significant reduction of vibrations around 100 Hz and a slight increase at 4.5 kHz. Without active phase control an overall reduction of phase noise of 20 % to 30 % was observed. In contrast, it only had a negligible effect on the phase noise with active phase control. Table 1 summarizes the $\mathrm{OPD_{rms}}$ values for both multipass amplifier setups in normal configuration (without rods) and stiffened configuration (connected with rods). Probably the reduction of phase noise within the control loop bandwidth and the increased amplitude of disturbances at greater frequencies compensated each other, resulting in similar $\mathrm{OPD_{rms}}$ values. Nonetheless $\mathrm{OPD_{rms}} = 15\ \mathrm{nm} = \lambda/69$ was achieved for one disk double pass.

Other active phase control setups reach residual phase noise figures from $\lambda/30$ [24] to $\lambda/80$ [25]. On the one hand this shows that simple mechanical setups (only one disk double pass) can be controlled with piezo actuators and achieve results comparable to setups using high-bandwidth electro-optic modulators. On the other hand with the number of disk passes phase noise increases up to $\mathrm{OPD_{rms}} = 116\ \mathrm{nm} = \lambda/9$ for four disk double passes. This poses a challenge for coherent

OSA CONTINUUM

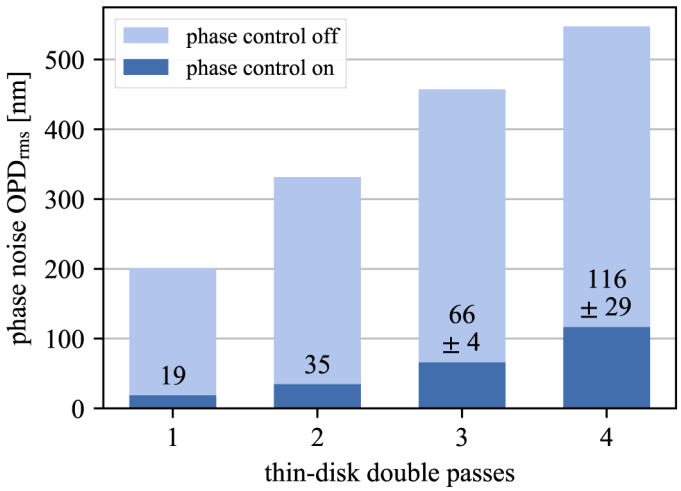

Fig. 5. Phase noise for multiple disk passes. For three and four double passes phase noise is given as the mean between OPD_{rms} values calculated from controller error and SDR measurement. Corresponding uncertainty intervals are given.

Table 1. Phase noise OPD_{rms} for one to four thin-disk double passes with active phase control through the two multipass setups (MP). Whenever measurements were distorted by the phase comparator an uncertainty interval is given. In the stiffened setup the mirror mounting rings are connected with rods.

		Phase noise OPD_{rms} [nm]			
number of disk double passes		1	2	3	4
MP 1	normal setup	19	35	66 ± 4	116 ± 29
MP 1	stiffened setup	15	38	65 ± 2	114 ± 28
MP 2	normal setup	27	51 ± 6	90 ± 15	—
MP 2	stiffened setup	24	52 ± 6	78 ± 9	90 ± 11

combining of multipass amplifiers in general and for thin-disk lasers in particular, where due to the low thickness of the disk multiple passes through the gain medium are necessary.

As described in Sec. 2.1 the second multipass setup (MP 2) is almost identical to the functional multipass amplifier. Instead of the Yb:YAG disk a mirror is mounted on the heat sink. However, a comparison between the 6 mm thick mirror and a 200 µm thin disk showed no difference regarding phase noise characteristics proving its validity as a replacement of a functional thin-disk amplifier. The multipass setups also differ with respect to the used piezo elements and electronic amplifiers. Network analysis of these components show that for small frequencies the electronic amplifier for MP 1 introduces less time delay than its counterpart for MP 2. For greater frequencies, however, the performance of the components in MP 2 is better. This fits the trend given in Table 1. For one disk double pass the performance of the control loop in MP 1 is better, whereas for four disk double passes lower phase noise is achieved in MP 2, due to the superior performance at higher frequencies. This means that the systems performance is largely influenced and in this case probably limited by the electronic amplifiers driving the phase shifting piezo elements.

The beam combination step demands to superimpose the beams on a beamsplitter with matching propagation directions. The combining efficiency η is the ratio of the combined beam's power in the desired output direction and the sum of the powers of the beams before combining.

OSA CONTINUUM

Considering only a phase difference of ϕ the combining efficiency for two beams is

$$\eta = \frac{1 + \cos\phi}{2} \approx 1 - \frac{\phi^2}{4}. \tag{2}$$

Since the phase noise of the amplifiers was measured separately, the specific phase difference at any point in time between their beams is unknown. But the spread of their phase differences over the course of the measurement interval can be assessed statistically. Each amplifier's phase noise is approximated as normally distributed with zero mean and a standard deviation of $\sigma_{\phi,i} = \mathrm{OPD}_{\mathrm{rms},i} \cdot 2\pi/\lambda$ with respect to the reference. The variance of their phase difference is

$$\sigma_\phi^2 = \sigma_{\phi,1}^2 + \sigma_{\phi,2}^2, \tag{3}$$

if the phase noise is assumed to be uncorrelated. This is of course a worst-case assumption, since both multipass amplifiers are mounted to the same optical table.

The time-averaged combining efficiency can be approximated by

$$<\eta> \approx 1 - \frac{\sigma_\phi^2}{4}. \tag{4}$$

Here σ_ϕ^2 describes the variance of the phase difference between both beams over the course of one second, that is to be expected given their individual phase noise characteristics $\mathrm{OPD}_{\mathrm{rms},i}$.

With the phase noise figures in Table 1 combining efficiencies from 0.99 to 0.8 for one to four disk double passes are to be expected. However, for one disk double pass a 41 mW and a 66 mW beam were combined into a 81 mW beam resulting in a combining efficiency of 0.75. The power imbalance is caused by the use of different beam samplers used for the heterodyne measurement. Considering this power imbalance alone, only a 1 % decrease in combining efficiency is to be expected [26]. Also with multiple disk double passes the combining efficiency was measured to be lower than expected ranging from 0.71 to 0.65 for two to four disk double passes respectively.

The lower than expected combining efficiency is probably caused by unmatched beam profiles. This became evident when investigating the combined beam's intensity profile. In the state of lowest output power it showed a dark center due to destructive interference surrounded by a bright ring of constructive interference. These inconstant interference states are an indication of different wavefront curvatures. They might have been caused by misadjusted collimating telescopes. In future experiments the beam profile difference can either be corrected statically by manually adjusting the telescope in one of the multipass setups or dynamically by implementing a second control loop, in which wavefront distortions are compensated. This would have the added benefit of also compensating distortions introduced by thermal lensing effects.

Another difference is that the combining efficiency drops by only 10 percentage points as the number of disk double passes increases instead of 20 as expected. This might be caused by correlated vibrations due to the amplifiers being coupled by the optical table.

By superimposing the two phase locked beams with slightly different propagation directions an interference pattern can be generated. The pattern's position is determined by the relative phase difference of the beams. By integrating over multiple interference pattern positions with a camera exposure time of one second, the varying phase differences between them yield an image of the interference pattern with lower visibility. Without phase control (top row in Fig. 6) the interference pattern vanishes due to greater phase noise as the number of disk passes increases. In contrast, with phase control the pattern remains visible, confirming the established coherence between both beams.

Finally, possible improvements based on the findings reported in this study are proposed. These cover ways to increase output power and to decrease phase noise. The amplifying characteristics, mainly the extraction efficiency, of the thin-disk amplifier can be improved by using a seed laser

OSA CONTINUUM

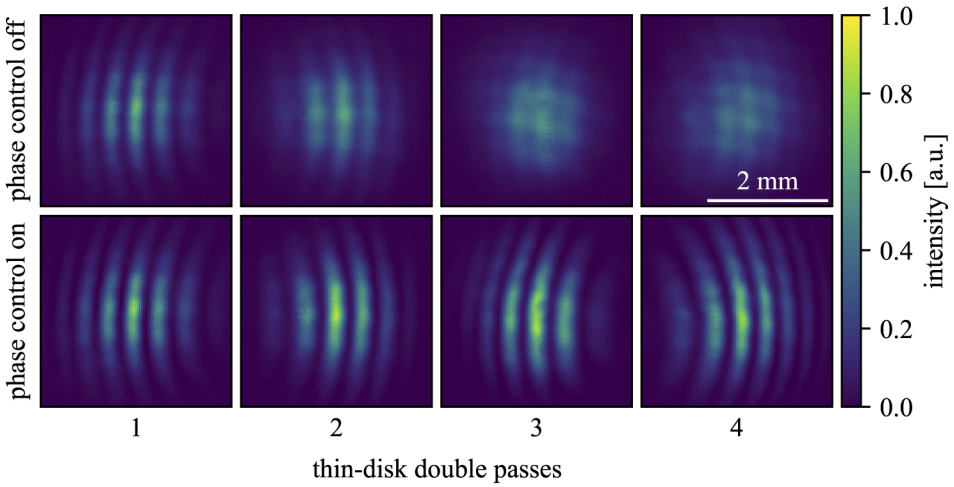

Fig. 6. Interference pattern between the two beams after one to four thin-disk double passes. Exposure time of 1 s. With activated phase control the interference pattern remains visible, which is particularly apparent for multiple passes through the laser disk.

with greater power or pre-amplification of said. One requirement for such a device is frequency stability to enable a stable heterodyne measurement. The amplifiers gain can be enhanced by increasing the number of disk passes. To make this possible a different cooling approach could be used to reduce mechanical vibrations. The electronic amplifiers driving the phase shifters can be optimized to increase the control bandwidth. Additionally, the multipass setup can be modified, for example by miniaturizing, to decrease phase noise. Power scaling is also achievable by combining more than two beams. Compared to the used setup, it would most certainly require the aforementioned miniaturizing of the multipass setup and another means of combining the beams, for example by a diffractive optical element or by arranging the beams side-by-side for combining with a tiled aperture approach.

4. Conclusion

We report on coherent combination of two beams passing through a multipass thin-disk laser amplifier and a similar multipass setup respectively. To our knowledge this is the first demonstration of coherently combined thin-disk lasers. Piezo mirrors are used to actively compensate phase noise, which is measured by heterodyne detection. The main source of phase noise are mechanical vibrations caused by the turbulent water cooling at the disk's rear side. The impact of this could be significantly reduced by a modified design, which makes use of a different cooling approach and an alternate mechanical realization of the multipass setup. In contrast, thermal effects by the pumping diodes are negligible. Phase noise increases with the number of disk passes posing a challenge for multipass amplifiers. For one thin-disk double pass a root mean square phase error of 15 nm = $\lambda/69$ has been achieved. After four double passes the phase error is about $\lambda/10$.

Disclosures

The authors declare no conflicts of interest.

References

1. A. Giesen, H. Hügel, A. Voss, K. Wittig, U. Brauch, and H. Opower, "Scalable concept for diode-pumped high-power solid-state lasers," Appl. Phys. B **58**(5), 365–372 (1994).

OSA CONTINUUM

2. T. Ryba, S. Zaske, S.-S. Schad, and A. Killi, "Latest advances in high power and high brightness laser technology," in "*Solid State Lasers XXVIII: Technology and Devices*," W. A. Clarkson and R. K. Shori, eds. (SPIE, 2019).
3. J. Mende, J. Speiser, G. Spindler, W. L. Bohn, and A. Giesen, "Mode dynamics and thermal lens effects of thin-disk lasers," in "*SPIE Proceedings Vol. 6871*," W. A. Clarkson, N. Hodgson, and R. K. Shori, eds. (2008), p. 68710M.
4. S. Nagel, B. Metzger, T. Gottwald, V. Kuhn, A. Killi, and S.-S. Schad, "Thin disk laser operating in fundamental mode up to a power of 4kW," in "*2019 Conference on Lasers and Electro-Optics Europe and European Quantum Electronics Conference*," (Optical Society of America, 2019), p. ca_5_4.
5. B. Shiner, "The impact and of fiber and laser technology and on the world and wide," in "*CLEO: Applications and Technology*," (Optical Society of America, 2013), pp. AF2J–1.
6. S. Ikoma, K. Uchiyama, Y. Takubo, M. Kashiwagi, K. Shima, and D. Tanaka, "5-kW single stage all-fiber Yb-doped single-mode fiber laser for materials processing," in *Fiber Lasers XV: Technology and Systems*, A. L. Carter and I. Hartl, eds. (SPIE, 2018).
7. F. Beier, C. Hupel, S. Kuhn, S. Hein, J. Nold, F. Proske, B. Sattler, A. Liem, C. Jauregui, J. Limpert, N. Haarlammert, T. Schreiber, R. Eberhardt, and A. Tünnermann, "Single mode 4.3 kW output power from a diode-pumped Yb-doped fiber amplifier," Opt. Express **25**(13), 14892 (2017).
8. C. X. Yu, O. Shatrovoy, T. Y. Fan, and T. F. Taunay, "Diode-pumped narrow linewidth multi-kilowatt metalized Yb fiber amplifier," Opt. Lett. **41**(22), 5202 (2016).
9. D. C. Brown and H. J. Hoffman, "Thermal, stress, and thermo-optic effects in high average power double-clad silica fiber lasers," IEEE J. Quantum Electron. **37**(2), 207–217 (2001).
10. T. Eidam, C. Wirth, C. Jauregui, F. Stutzki, F. Jansen, H.-J. Otto, O. Schmidt, T. Schreiber, J. Limpert, and A. Tünnermann, "Experimental observations of the threshold-like onset of mode instabilities in high power fiber amplifiers," Opt. Express **19**(14), 13218–13224 (2011).
11. M. N. Zervas and C. A. Codemard, "High power fiber lasers: A review," IEEE J. Sel. Top. Quantum Electron. **20**(5), 219–241 (2014).
12. T. Y. Fan, "Laser beam combining for high-power, high-radiance sources," IEEE J. Sel. Top. Quantum Electron. **11**(3), 567–577 (2005).
13. E. Shcherbakov, V. Fomin, A. Abramov, A. Ferin, D. Mochalov, and V. P. Gapontsev, "Industrial grade 100 kW power cw fiber laser," in "*Advanced Solid State Lasers*," (Optical Society of America, 2013), pp. ATh4A–2.
14. S. J. McNaught, C. P. Asman, H. Injeyan, A. Jankevics, A. M. Johnson, G. C. Jones, H. Komine, J. Machan, J. Marmo, M. McClellan, R. Simpson, J. Sollee, M. M. Valley, M. Weber, and S. B. Weiss, "100-kW coherently combined Nd:YAG MOPA laser array," in "*Frontiers in Optics 2009/Laser Science XXV/Fall 2009 OSA Optics & Photonics Technical Digest*," (OSA, 2009).
15. M. Müller, C. Aleshire, A. Klenke, E. Haddad, F. Légaré, A. Tünnermann, and J. Limpert, "10.4 kW coherently combined ultrafast fiber laser," Opt. Lett. **45**(11), 3083 (2020).
16. J. Pouysegur, B. Weichelt, F. Guichard, Y. Zaouter, C. Hönninger, E. Mottay, F. Druon, and P. Georges, "Simple Yb:YAG femtosecond booster amplifier using divided-pulse amplification," Opt. Express **24**(9), 9896–9904 (2016).
17. M. Kienel, M. Müller, S. Demmler, J. Rothhardt, A. Klenke, T. Eidam, J. Limpert, and A. Tünnermann, "Coherent beam combination of Yb:YAG single-crystal rod amplifiers," Opt. Lett. **39**(11), 3278–3281 (2014).
18. D. N. Papadopoulos, F. Friebel, A. Pellegrina, M. Hanna, P. Camy, J. Doualan, R. Moncorgé, P. Georges, and F. P. H. J. Druon, "High repetition rate Yb:CaF2 multipass amplifiers operating in the 100-mj range," IEEE J. Sel. Top. Quantum Electron. **21**(1), 464–474 (2015).
19. J. Speiser, "Thin disk lasers: history and prospects," in "*Procedings Volume 9893*," J. I. Mackenzie, H. JelÍnková, T. Taira, and M. A. Ahmed, eds. (International Society for Optics and Photonics, 2016), p. 98930L.
20. M. S. Fadali and A. Visioli, *Digital control engineering: Analysis and design* (Academic Press, Waltham, 2013), 2nd ed.
21. A. Retzler, "SDR-Lab: An RTL-SDR interface to LabVIEW for educational purposes," (2016).
22. O. Mężyk, M. Doligalski, and R. Rybski, "Measurements of signal delays in software defined radio with use of gnss modules," Ann. Navig. **26**(1), 98–105 (2019).
23. G. D. Goodno, L. D. Book, J. E. Rothenberg, M. E. Weber, and S. B. Weiss, "Narrow linewidth power scaling and phase stabilization of 2-μm thulium fiber lasers," Opt. Eng. **50**(11), 111608 (2011).
24. G. D. Goodno, C. P. Asman, J. Anderegg, S. Brosnan, E. C. Cheung, D. Hammons, H. Injeyan, H. Komine, W. H. Long, M. McClellan, S. J. McNaught, S. Redmond, R. Simpson, J. Sollee, M. Weber, S. B. Weiss, and M. Wickham, "Brightness-scaling potential of actively phase-locked solid-state laser arrays," IEEE J. Sel. Top. Quantum Electron. **13**(3), 460–472 (2007).
25. G. D. Goodno, S. J. McNaught, J. E. Rothenberg, T. S. McComb, P. A. Thielen, M. G. Wickham, and M. E. Weber, "Active phase and polarization locking of a 1.4 kW fiber amplifier," Opt. Lett. **35**(10), 1542–1544 (2010).
26. T. Y. Fan, "The effect of amplitude (power) variations on beam combining efficiency for phased arrays," IEEE J. Sel. Top. Quantum Electron. **15**(2), 291–293 (2009).